

Localization and universal fluctuations in ultraslow diffusion processes

Aljaž Godec,^{1,2} Aleksei V. Chechkin,^{3,4,1} Eli Barkai,⁵ Holger Kantz,⁴ and Ralf Metzler^{1,6}

¹*Institute for Physics & Astronomy, University of Potsdam, 14476 Potsdam-Golm, Germany*

²*National Institute of Chemistry, 1000 Ljubljana, Slovenia*

³*Institute for Theoretical Physics, Kharkov Institute of Physics and Technology, Kharkov 61108, Ukraine*

⁴*Max-Planck Institute for the Physics of Complex Systems, Nöthnitzer Straße 38, 01187 Dresden, Germany*

⁵*Department of Physics, Bar Ilan University, Ramat-Gan 52900, Israel*

⁶*Department of Physics, Tampere University of Technology, FI-33101 Tampere, Finland*

We study ultraslow diffusion processes with logarithmic mean squared displacement (MSD) $\langle x^2(t) \rangle \simeq \log^\gamma t$. Comparison of annealed continuous time random walks (CTRWs) with logarithmic waiting time distribution $\psi(\tau) \simeq 1/(\tau \log^{1+\gamma} \tau)$ and Sinai diffusion in quenched random landscapes shows striking similarities, despite their very different physical nature. In particular, they exhibit a weakly non-ergodic disparity of the time and ensemble averaged MSDs. Remarkably, for the CTRW we observe that the fluctuations of time averages become universal with an exponential suppression of mobile trajectories. We discuss the fundamental connection between the Golosov localization effect and non-ergodicity in the sense of the disparity between ensemble and time averaged MSD.

PACS numbers: 72.20.Jv, 72.70.+m, 89.75.Da, 05.40.-a

Ever since Karl Pearson's defining letter to the editor 1905 [1] as well as Einstein's and Smoluchowski's mean free path studies [2], *random walks* have become a standard approach to a multitude of nonequilibrium phenomena across disciplines [3–5]. Most frequently renewal random walks are used [5] in which jumps are independent of previous jumps, reflecting the motion in annealed environment [6]. These contrast random walks in quenched environments in which a particle progressively builds up correlations when it returns to previously visited locations with site-specific properties [6]. The prototype approach is Temkin's lattice model with site-dependent probabilities for jumping left or right [3, 7].

A great leap forward came with Sinai's study of a special case of Temkin's model in which a walker jumps from site x to $x \pm 1$ with the site-specific probability $p_x = \frac{1}{2}(1 \pm \varepsilon s_x)$ [8]. Here, the amplitude $0 < \varepsilon < 1$ and $s_x = \pm 1$ with probability $1/2$ [3, 9]. Sinai diffusion can be viewed as a random walk in the quenched potential landscape created by a standard random walk. A simple argument for the temporal spreading in Sinai diffusion goes as follows [6]. To span a distance x from its starting point the particle needs to cross an energy barrier of order \sqrt{x} with activation time $\tau \sim \tau_1 \exp(\sigma\sqrt{x})$, where σ is a measure for the disorder strength versus thermal energy and τ_1 a fundamental time scale. The distance covered by the walker during time t then scales as $x^2 \simeq \ln^4(t/\tau_1)$.

Sinai diffusion is related to the random-field Ising model [10, 11] and helix-coil phase boundaries in random heteropolymers [12]. In a biophysical context, due to the inherently quenched heterogeneity of biomolecules Sinai-type models are used to describe mechanical DNA unzipping [13], translocation of biomolecules through nanopores [14, 15], and molecular motor motion [15]. Ultraslow diffusion with mean squared displacement (MSD)

$$\langle x^2(t) \rangle \simeq 2K_\gamma \ln^\gamma t, \quad \gamma > 0 \quad (1)$$

in fact has a much broader scope in highly disordered low-dimensional systems: inter alia, in vacancy induced motion [16, 17], biased motion in exclusion processes [18], motion in aging environments [19], compactification of paper [20] or grain [21], dynamics in glassy systems [22], record statistics [23], the ABC model [24], diffusion with exponential position dependence of the diffusivity [25], or dynamics in non-linear maps [26].

Here we report a comparative study of Sinai diffusion and ultraslow continuous time random walks (CTRWs) with super heavy-tailed waiting times [26–29]. Previous work focused on ensemble averaged observables. The routine observation of single particle trajectories in the laboratory forces us to investigate time averages theoretically. Here we study the time averaged MSD of Sinai and ultraslow CTRW and demonstrate the fundamental disparity between ensemble and time averages. This weakly non-ergodic behavior [30, 31] is, up to a prefactor, identical for both processes. We discuss why, despite the seeming similarity, the problem of ergodicity in annealed and quenched systems is very different. In addition, we unveil the *universal* exponential fluctuations of the time averaged MSD of the CTRW process and provide numerical evidence of the Golosov localization effect for different disorder realizations in Sinai diffusion. Concurrently, the PDF of the CTRW process is shown to be practically indistinguishable from that of Sinai diffusion.

Sinai diffusion. We start with the analysis of Sinai diffusion. In the continuum limit its MSD reads [10, 32]

$$\widetilde{\langle x^2(t) \rangle} \simeq \frac{61}{180} \ln^4(t), \quad (2)$$

in scaled units. Here $\langle \cdot \rangle$ is an ensemble average over white Gaussian noise and $\widetilde{\cdot}$ a disorder average. Fig. 1 shows excellent agreement with our extensive simulations.

To simulate Sinai diffusion, we follow the approach of Ref. [32] based on a discrete-space Fokker Planck equa-

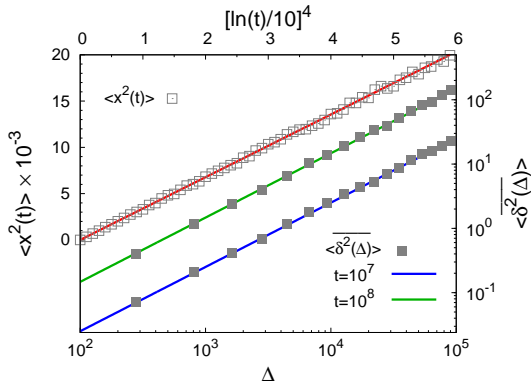


FIG. 1: Ensemble averaged (\square , top and left axes) and time averaged (\blacksquare , bottom and right axes, for $t = 10^7$ and $t = 10^8$) MSD of Sinai diffusion. The simulations agree excellently with the analytical results (full lines) of Eqs. (2) and (7). Note that we show $10^{-3}\langle x^2(t) \rangle$ such that for sufficiently long trajectories [long t in Eq. (7)] $\langle x^2 \rangle \gg \overline{\delta^2}$.

tion for a particular realization of the random potential. Mapping the Fokker Planck equation onto the corresponding (imaginary time) Schrödinger equation, we obtain the propagator as an expansion in eigenstates from diagonalization of the Schrödinger operator. From the disorder-averaged one-point and two-point propagators we evaluate the time and ensemble averaged MSDs (see also below). Results were averaged over 5000 realizations of the random potential with 10^8 time steps each [33].

Individual time series $x(t)$ garnered by modern single particle tracking techniques or from simulations are typically evaluated in terms of the time averaged MSD [30]

$$\overline{\delta^2(\Delta)} = \frac{1}{t - \Delta} \int_0^{t-\Delta} [x(t' + \Delta) - x(t')]^2 dt', \quad (3)$$

with the lag time Δ and the length t of the time series. The overline $\overline{\quad}$ denotes the time average. Averaging Eq. (3) over many trajectories embedded in different realizations of the disorder we have

$$\begin{aligned} \overline{\langle \delta^2(\Delta) \rangle} &\sim \frac{1}{t - \Delta} \int_0^{t-\Delta} [\langle x^2(t' + \Delta) \rangle + \langle x^2(t') \rangle \\ &\quad - 2\langle x(t')x(t' + \Delta) \rangle] dt' \end{aligned} \quad (4)$$

where the two-point position correlation function

$$\langle x(t')x(t' + \Delta) \rangle = \sqrt{\langle x^2(t' + \Delta) \rangle \langle x^2(t') \rangle} f(y) \quad (5)$$

is known from renormalization group calculations by Le Doussal et al. [32], where $y = \ln(t' + \Delta)/\ln t'$ and

$$\begin{aligned} f(y) &= \frac{72}{61y} - \frac{40}{61y^2} - \frac{180}{427y^3} + \frac{2045}{1281y^4} \\ &\quad + e^{y-1} \left(\frac{20}{61y^2} - \frac{80}{183y^3} - \frac{36}{61y^4} \right). \end{aligned} \quad (6)$$

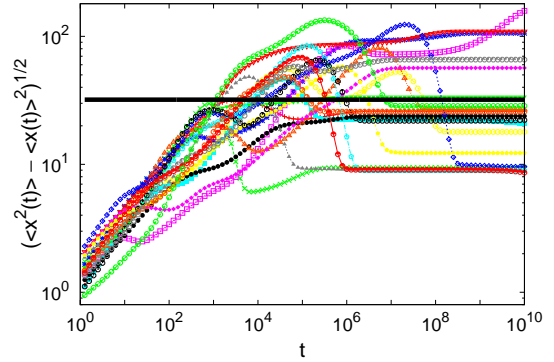


FIG. 2: Standard deviation $[\langle x^2(t) \rangle - \langle x(t) \rangle^2]^{1/2}$ for individual realizations of the quenched potential landscape in the Sinai model. The universal localization due to the Golosov effect is distinct. The horizontal black line shows the value 32.

Inserting into Eq. (4) we obtain our first main result, the time averaged MSD

$$\overline{\langle \delta^2(\Delta) \rangle} \simeq \frac{3721}{17080} \ln^4(t) \frac{\Delta}{t} = \overline{\langle x^2(t) \rangle} \frac{549}{854} \frac{\Delta}{t}, \quad (7)$$

up to corrections of order $(\Delta/t)^2$ [33]. In Eq. (7) we observe the distinct disparity between the MSD (2) and its time averaged analog (7). In contrast to the logarithmic time dependence (2) for the MSD, the time averaged MSD (7) grows *linearly* with the lag time Δ . Concurrently, it displays the aging dependence proportional to $\ln^4(t)/t$, i.e., the process is progressively slowed down. Physically, this is effected when the random walker hits increasingly deeper wells. In Fig. 1 without fit we see excellent agreement between the analytical prediction (7) and the simulations, including the dependence on t .

However, when discussing time averages in non-trivial quenched systems such as Sinai landscape, we must distinguish between at least two averaging scenarios. In the first case each path is realized on its own unique quenched landscape, and after averaging the individual time averaged MSDs $\overline{\delta^2}$ over disorder we get Eq. (7). Second, we can consider one unique disordered system with an ensemble of non-interacting particles which all start at the origin. The thermal noise for each particle is independent. Still, in the long time limit we can expect that the time averaged MSD for all particles will depend on the specific realization of the disorder, and due to the Golosov localization effect all trajectories will yield similar values for the time averaged MSD. Hence we now focus on the Golosov effect [34]: In a given realization of the disorder the ratio $\langle x(t) \rangle / \ln^2 t$ for a fixed initial position up to a prefactor of order unity becomes deterministic: the particles get stuck in the deepest potential minimum they can reach within the time t . In particular, for the standard deviation the result $[\langle x^2(t) \rangle - \langle x(t) \rangle^2]^{1/2} \simeq 32$ in scaled units was obtained [34]. Fig. 2 demonstrates that indeed a universal localization of this MSD emerges.

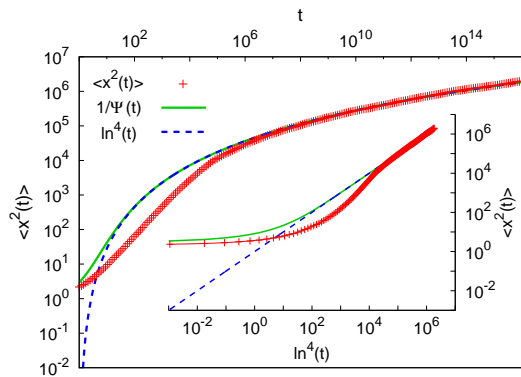


FIG. 3: MSD $\langle x^2(t) \rangle$ of the CTRW ($\gamma = 4$, $\tau_0 = e$, $\langle \delta x^2 \rangle = 1$ used for all CTRW plots). Main graph: log-log scales. Inset: $\langle x^2(t) \rangle$ versus $\ln^4(t)$ with linear asymptote.

The variations of the onset and height of the plateaus in Fig. 2 reflect different realizations of the disorder. An important feature of Sinai diffusion is the slow convergence to the Golosov localization, found after 10^4 to 10^5 time steps. The numerical analysis of the Golosov effect in different disorder realizations is our second main result.

Ultraslow CTRW. In contrast to systems with quenched disorder, those with annealed disorder typically allow for a rigorous treatment. It would therefore be desirable to have a process, that captures the essential features of the Sinai diffusion. We show that such a process is given by a renewal CTRW on a one-dimensional lattice with the asymptotic form $\psi(\tau) \sim h(\tau)/\tau$ of the distribution of waiting times τ elapsing between successive jumps [29]. Here $h(\tau)$ is a slowly varying function [35]. Jumps to left and right are equally likely, and the probability that no jump occurs until time t is $\Psi(t) = \int_t^\infty \psi(\tau) d\tau$, in terms of which we express our results. A typical example is the logarithmic form [26–29]

$$\Psi(t) = \ln^\gamma(\tau_0) / \ln^\gamma(\tau_0 + t), \quad (8)$$

where $\tau_0 > 0$ avoids a divergence at $t = 0$. The MSD is given by $\langle x^2(t) \rangle \sim \langle \delta x^2 \rangle / \Psi(t)$ [33], where $\langle \delta x^2 \rangle$ is the variance of jump lengths [36]. The specific form (8) recovers the MSD (1) with diffusivity $K_\gamma = \langle \delta x^2 \rangle / [2 \ln^\gamma(\tau_0)]$ [26, 27, 29, 37], i.e., for $\gamma = 4$, we find a Sinai-like diffusion. Fig. 3 demonstrates the convergence of the simulations to the predicted logarithmic behavior. The agreement, including the prefactor, after some 10^6 steps becomes excellent. In the inset of Fig. 3 we show the linear asymptotic scaling of $\langle x^2(t) \rangle$ as function of $\ln^4(t)$.

To obtain the time averaged MSD for this ultraslow CTRW process we note that the MSD (1) can be rewritten as $\langle x^2(t) \rangle = \langle \delta x^2 \rangle \langle n(t) \rangle$ in terms of the average number of jumps $\langle n(t) \rangle$ of the random walker from $t = 0$ up to time t , and thus $\langle n(t) \rangle \sim 1/\Psi(t)$. For the calculation of $\overline{\langle \delta^2 \rangle}$ we need the correlation function $\langle [x(t' + \Delta) - x(t')]^2 \rangle$ [see Eq. (3)]. As individual jumps are independent ran-

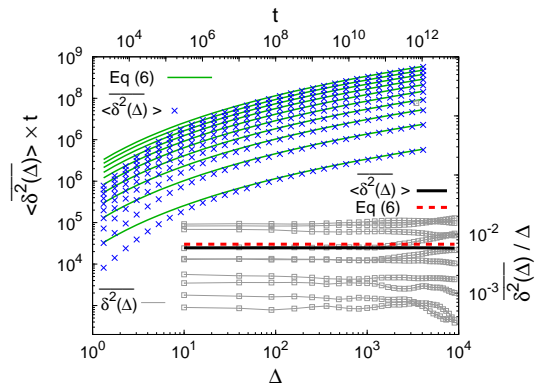


FIG. 4: Numerical results for $\overline{\langle \delta^2 \rangle} \times t$ of the CTRW versus t for $\Delta = 20$ to 200 in steps of 20 (\times , bottom to top). Lines show Eq. (9), without adjustable parameter. Bottom right: $\overline{\langle \delta^2 \rangle} / \Delta$ versus lag time Δ with $t = 10^7$ for ten different realizations, showing distinct amplitude scatter. Thick lines represent Eq. (9) and the average $\overline{\langle \delta^2 \rangle}$ of the plotted realizations.

dom variables with zero mean, $\langle [x(t' + \Delta) - x(t')]^2 \rangle = \langle \delta x^2 \rangle [\langle n(t' + \Delta) \rangle - \langle n(t') \rangle]$. The time averaged MSD then is $\overline{\langle \delta^2 \rangle} \simeq \langle \delta x^2 \rangle \Delta / [t \Psi(t)]$. For the form (8) we have

$$\overline{\langle \delta^2 \rangle} \sim \langle x^2(t) \rangle \Delta / t : \quad (9)$$

Ultraslow CTRWs exhibit weak ergodicity breaking with a linear Δ -dependence, similar to CTRWs with a power-law form for $\psi(\tau)$ [30, 38, 39] and other processes [40–42]. In particular, Eq. (9), up to the numerical factor $549/854$, equals the relation (7) between $\langle x^2 \rangle$ and $\overline{\langle \delta^2 \rangle}$ for the disorder-averaged Sinai diffusion. This similarity is our third main result.

In Fig. 4 we plot results from our simulations for the time averaged MSD, demonstrating the convergence of the numerical results to the expression (9) as function of the length t of the time series. Fig. 4 also depicts the time averaged MSD as function of the lag time Δ for 10 individual realizations along with the result (9) for the mean behavior. A significant amplitude variation is observed between the individual realizations. This implies that, unlike for Brownian motion, the experimental observation of a single trajectory producing $\overline{\langle \delta^2 \rangle}$ does not provide the full information on neither $\langle x^2 \rangle$ nor $\overline{\langle \delta^2 \rangle}$.

Time averages of physical observables such as the MSD (3) in weakly non-ergodic systems remain random variables even in the limit of long measurement times but have a well-defined distribution [30, 38, 39, 43]. To derive these fluctuations for the ultraslow CTRW process in terms of the dimensionless variable $\xi = \overline{\langle \delta^2 \rangle} / \langle \delta^2 \rangle$, we make use of the relation $\overline{\langle \delta^2 \rangle}(\Delta) / \langle \delta^2 \rangle(\Delta) = n(t) / \langle n(t) \rangle$ [39, 44] and invoke the probability for the occurrence of n jumps up to time t , $p_n(s) = [1 - \psi(\tau)] s^{-1} \exp\{n \ln[\psi(s)]\}$ in Laplace space [3, 45]. For the latter, after Laplace inversion we get $p_n(t) \sim \Psi(t) \exp\{-n \Psi(t)\}$. Finally, after

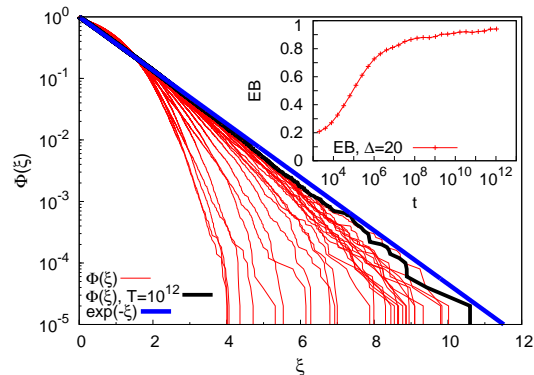


FIG. 5: The amplitude scatter distribution $\phi(\xi)$ versus $\xi = \overline{\delta^2}/\langle\delta^2\rangle$ for $\Delta = 500$ and increasing t successively approaches the exponential (10) shown by the full line, compare the realization with $t = 10^{12}$. Inset: convergence $EB \rightarrow 1$ of the ergodicity breaking parameter versus t for $\Delta = 20$.

change of variables, $\phi(\xi) = p_n(\xi) \times dn/d\xi$, we arrive at the exponential form for the distribution of time averages

$$\lim_{t \rightarrow \infty} \phi(\xi) \sim \exp(-\xi). \quad (10)$$

Remarkably this result is universal in the sense that it is valid for any generic ultraslow waiting time distribution $\psi(\tau) \sim h(\tau)/\tau$. In particular, it is independent of the exponent γ . The maximum of this distribution is at $\xi = 0$, i.e., many realizations of the ultraslow CTRW process do not perform any jump. Trajectories with many jumps and thus larger ξ values are exponentially suppressed. The ergodicity breaking parameter [39] is $EB = \lim_{t \rightarrow \infty} \langle \xi^2 \rangle - 1 = 1$. The universal fluctuations of ultraslow CTRWs are another central result. For Sinai diffusion this point remains open, as the simulations methods do not allow us to obtain sufficiently long and many single trajectories to analyze their amplitude fluctuations. The results for the Golosov effect (Fig. 2) show that the simulations times are beyond our reach.

Similarity of the PDFs. We would expect that the PDF $P(x, t)$ is more sensitive to the deep differences between CTRW and Sinai diffusion. Fig. 6 shows good convergence of the numerical data to the Sinai PDF [46, 47]

$$\widetilde{P}(x, t) \sim \frac{4}{\pi^2 \ln^2(t)} \sum_{n=0}^{\infty} \frac{(-1)^n}{2n+1} \exp\left(-\frac{(2n+1)^2 \pi^2 |x|}{4 \ln^2(t)}\right) \quad (11)$$

for increasing t . At all times, the zeroth term of this series contributes ≈ 0.33 to the normalization. Higher order, alternating terms effect a distinct central plateau, while the wings of the PDF (11) are dominated by the zeroth term. The numerical results nicely corroborate the flat center region of the PDF, which is physically due to the local bias of the Sinai diffusion at each site effecting the small depletion at the origin. In Fig. 6 we compare the

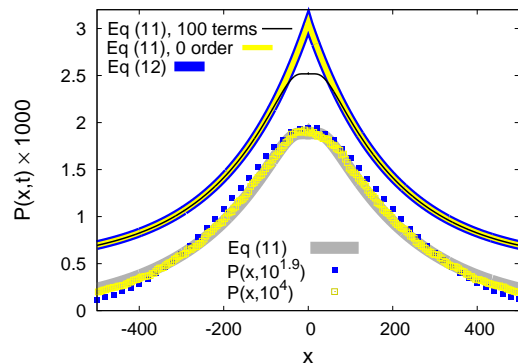


FIG. 6: PDF (11) of Sinai diffusion (thick gray line) with numerical results for two times (■ and □), showing good convergence. Shifted curves (top): Rescaled PDF (12) of ultraslow CTRW (thick blue line) with zero order term of the Sinai PDF (11) (medium yellow line) and result (11) with 100 terms (thin black line), showing perfect agreement of the tails.

PDF (11) with the CTRW PDF [26, 27, 29]

$$P(x, t) \sim \sqrt{\Psi(t)/[2\langle\delta x^2\rangle]} \exp\left\{-|x| \sqrt{2\Psi(t)/\langle\delta x^2\rangle}\right\}. \quad (12)$$

Being interested in the qualitative comparison of CTRW and Sinai diffusion in Eq. (11) we rescale the zero order term with a factor of order unity such that it is identical to the PDF (12) with its distinct cusp at the origin. Fig. 6 shows that the full result (11) perfectly matches the tails of the CTRW PDF (12). In the analysis of experimental data the PDFs of both processes will be practically indistinguishable unless very accurate data are available.

Conclusions. Sinai diffusion and ultraslow renewal CTRW are two fundamentally different processes: the former takes place in a quenched random potential, the latter in an annealed environment. Despite this difference, both exhibit identical logarithmic scaling of the ensemble MSD and exhibit weak ergodicity breaking: their time averaged MSD scales linearly with the lag time Δ and explicitly depends on the process time t in a characteristic way. We pointed to the deep connection between the Golosov phenomenon and ergodicity breaking, a topic that demands rigorous mathematical treatment. The fluctuations of the amplitude of the time averaged MSD for the ultraslow annealed model exhibit a remarkable universality: in individual trajectories extended motion recorded in terms of the time averaged MSD is exponentially suppressed and details of the waiting time distribution do not matter. For Sinai diffusion this point remains open as sufficient statistics are beyond current computational reach.

We acknowledge funding from the Academy of Finland (FiDiPro scheme to RM), Alexander von Humboldt Foundation (AG), and Israel Science Foundation (EB).

-
- [1] K. Pearson, *Nature* **72**, 294 (1905).
- [2] A. Einstein, *Ann. d. Physik* **17**, 549 (1905); **19**, 371 (1906); M. von Smoluchowski, *Ann. d. Physik* **21**, 756 (1906).
- [3] B. D. Hughes, *Random Walks and Random Environments*, Vols. I and II (Oxford University Press, Oxford, UK, 1995).
- [4] D. Sornette, *Critical phenomena in natural sciences* (Springer, Berlin, 2006).
- [5] R. G. Gallager, *Stochastic processes: theory for applications* (Cambridge University Press, Cambridge, UK, 2013). K. V. Miltov and E. Omney, *Renewal processes* (Springer, Berlin, 2014).
- [6] J.-P. Bouchaud and A. Georges, *Phys. Rep.* **195**, 127 (1990); J.-P. Bouchaud, A. Comtet, A. Georges, and P. Le Doussal, *Ann. Phys. (N.Y.)* **201**, 285 (1990).
- [7] D. E. Temkin, *Sov. Math. Dokl.* **13**, 1172 (1972).
- [8] Ya. G. Sinai, *Theory Prob. Appl.* **27**, 256 (1982).
- [9] G. Oshanin, A. Rosso, and G. Schehr, *Phys. Rev. Lett.* **110**, 100602 (2013); D. S. Dean et al, E-print arXiv:1406.2612.
- [10] D. S. Fisher, P. Le Doussal, and C. Monthus, *Phys. Rev. E* **64**, 066107 (2001).
- [11] R. Bruinsma and G. Aeppl, *Phys. Rev. Lett.* **52**, 1547 (1984).
- [12] P. G. de Gennes, *J. Stat. Phys.* **12**, 463 (1975); G. Oshanin and S. Redner, *Europhys. Lett.* **85**, 10008 (2009).
- [13] J.-C. Waler, A. Ferrantini, E. Carlon, and C. Vanderzande, *Phys. Rev. E* **85**, 031120 (2012); Y. Kafri and A. Polkovnikov, *Phys. Rev. Lett.* **97**, 208104 (2006).
- [14] J. Mathé et al, *Biophys. J.* **87**, 3205 (2004); D. K. Lubensky, and D. R. Nelson, *ibid.* **77**, 1824 (1999).
- [15] Y. Kafri, D. K. Lubensky, and D. R. Nelson, *Biophys. J.* **86**, 3373 (2004).
- [16] M. J. A. Brummelhuis and H. J. Hilhorst, *J. Stat. Phys.* **53**, 249 (1988).
- [17] O. Bénichou and G. Oshanin, *Phys. Rev. E* **66**, 031101 (2002).
- [18] R. Juhász, L. Santen, and F. Iglói, *Phys. Rev. Lett.* **94**, 010601 (2005).
- [19] M. A. Lomholt, L. Lizana, R. Metzler, and T. Ambjörnsson, *Phys. Rev. Lett.* **110**, 208301 (2013).
- [20] K. Matan, R. B. Williams, T. A. Witten, and S. R. Nagel, *Phys. Rev. Lett.* **88**, 076101 (2002).
- [21] P. Richard, M. Nicodemi, R. Delannay, P. Ribière, and D. Bideau, *Nature Mat.* **4**, 121 (2005).
- [22] S. Boettcher and P. Sibani, *J. Phys. Cond. Mat.* **23**, 065103 (2011).
- [23] B. Schmittmann and R. K. P. Zia, *Am. J. Phys.* **67**, 1269 (1999).
- [24] N. Afzal and M. Pleimling, *Phys. Rev. E* **87**, 012114 (2013).
- [25] A. G. Cherstvy and R. Metzler, *Phys. Chem. Chem. Phys.* **15**, 20220 (2013).
- [26] J. Dräger and J. Klafter, *Phys. Rev. Lett.* **84**, 5998 (2000).
- [27] S. Havlin and G. H. Weiss, *J. Stat. Phys.* **58**, 1267 (1990).
- [28] A. V. Chechkin, J. Klafter, and I. M. Sokolov, *Europhys. Lett.* **63**, 326 (2003).
- [29] S. Denisov and H. Kantz, *Phys. Rev. E* **83**, 041132 (2011); S. I. Denisov, S. B. Yuste, Yu. S. Bystrik, H. Kantz, and K. Lindenberg, *ibid.* **84**, 061143 (2011).
- [30] E. Barkai, Y. Garini, and R. Metzler, *Phys. Today* **65**(8), 29 (2012).
- [31] J.-P. Bouchaud, *J. Phys. I (Paris)* **2**, 1705 (1992).
- [32] P. Le Doussal, C. Monthus, and D. S. Fisher, *Phys. Rev. E* **59**, 4795 (1999).
- [33] A. V. Chechkin, A. Godec, R. Metzler, H. Kantz, and E. Barkai (unpublished).
- [34] K. Golosov, *Commun. Math. Phys.* **92**, 491 (1984).
- [35] That is, $h(\mu\tau) \sim h(\tau)$ as $\tau \rightarrow \infty$ for $\mu > 0$. For instance, $h(\tau) \sim 1/\ln^\gamma(\tau)$ with $\gamma > 0$.
- [36] R. Metzler and J. Klafter, *Phys. Rep.* **339**, 1 (2000).
- [37] We choose the values $\langle \delta x^2 \rangle = 1$ and $\tau_0 = e$.
- [38] A. Lubelski, I. M. Sokolov, and J. Klafter, *Phys. Rev. Lett.* **100**, 250602 (2008); M. Khoury, A. M. Lacasta, J. M. Sancho, and K. Lindenberg, *ibid.* **106**, 090602 (2011); I. M. Sokolov, E. Heinsalu, P. Hänggi, and I. Goychuk, *Europhys. Lett.* **86**, 30009 (2009); M. Magdziarz and A. Weron, *Phys. Rev. E* **84**, 051138 (2011); T. Albers and G. Radons, *EPL* **102**, 40006 (2013).
- [39] Y. He, S. Burov, R. Metzler, and E. Barkai, *Phys. Rev. Lett.* **101**, 058101 (2008); S. Burov, J.-H. Jeon, R. Metzler, and E. Barkai, *Phys. Chem. Chem. Phys.* **13**, 1800 (2011).
- [40] A. G. Cherstvy, A. V. Chechkin, and R. Metzler, *New J. Phys.* **15**, 083039 (2013); *Soft Matter* **10**, 1591 (2014); P. Massignan et al, *Phys. Rev. Lett.* **112**, 150603 (2014); A. Fulinski, *J. Chem. Phys.* **138**, 021101 (2013); *Phys. Rev. E* **83**, 061140 (2011).
- [41] F. Thiel and I. M. Sokolov, *Phys. Rev. E* **89**, 012115 (2014); J.-H. Jeon, A. V. Chechkin, and R. Metzler, *Phys. Chem. Chem. Phys.* DOI: 10.1039/C4CP02019G; T. Miyaguchi and T. Akimoto, *Phys. Rev. E* **83**, 031926 (2011).
- [42] V. Tejedor and R. Metzler, *J. Phys. A* **43**, 082002 (2010); M. Magdziarz, R. Metzler, W. Szczotka, and P. Zebrowski, *Phys. Rev. E* **85**, 051103 (2012).
- [43] G. Bel and E. Barkai, *Phys. Rev. Lett.* **94**, 240602 (2005); A. Rebenshtok and E. Barkai, *J. Stat. Phys.* **133**, 565 (2008).
- [44] J. Schulz, E. Barkai, and R. Metzler, *Phys. Rev. Lett.* **110**, 020602 (2013); *Phys. Rev. X* **4**, 011028 (2014).
- [45] The Laplace transform $f(s) = \mathcal{L}\{f(t); t \rightarrow s\} = \int_0^\infty f(t) \exp(-st) dt$ of a function $f(t)$ is denoted by explicit dependence on the Laplace variable s .
- [46] A. Comtet and D. S. Dean, *J. Phys. A* **31**, 8595 (1998); see also H. Kesten, *Physica A* **138**, 299 (1986).
- [47] M. Nauenberg, *J. Stat. Phys.* **41**, 803 (1985); A. Bunde, S. Havlin, H. E. Roman, G. Schildt, and H. E. Stanley, *J. Stat. Phys.* **50**, 1271 (1988).